



Originally published as:

Luo, X., Xiong, C., Gu, S., Lou, Y., Stolle, C., Xin, W., Liu, K., Song, W. (2019): Geomagnetically Conjugate Observations of Equatorial Plasma Irregularities From Swarm Constellation and Ground-Based GPS Stations. - *Journal of Geophysical Research*, 124, 5, pp. 3650—3665.

DOI: <http://doi.org/10.1029/2019JA026515>

JGR Space Physics

RESEARCH ARTICLE

10.1029/2019JA026515

Key Points:

- The Swarm in situ electron density occasionally shows equatorial plasma irregularities at only one hemisphere
- The scintillations caused by equatorial plasma irregularities observed by two geomagnetically conjugate ground stations agree well with each other
- The different onset time of scintillation at two conjugate stations indicates the asymmetry features of EPIs along the flux tube

Correspondence to:

S. Gu and Y. Lou,
gsf@whu.edu.cn;
ydlou@whu.edu.cn

Citation:

Luo, X., Xiong, C., Gu, S., Lou, Y., Stolle, C., Wan, X., et al. (2019). Geomagnetically conjugate observations of equatorial plasma irregularities from Swarm constellation and ground-based GPS stations. *Journal of Geophysical Research: Space Physics*, 124, 3650–3665. <https://doi.org/10.1029/2019JA026515>






Received 17 JAN 2019

Accepted 18 APR 2019

Accepted article online 25 APR 2019

Published online 13 MAY 2019

Geomagnetically Conjugate Observations of Equatorial Plasma Irregularities From Swarm Constellation and Ground-Based GPS Stations

Xiaomin Luo¹, Chao Xiong² , Shengfeng Gu¹ , Yidong Lou¹ , Claudia Stolle^{2,3} , Xin Wan⁴ , Kangkang Liu⁵ , and Weiwei Song¹

¹GNSS Research Centre, Wuhan University, Wuhan, China, ²GFZ German Research Centre for Geosciences, Potsdam, Germany, ³Faculty of Science, University of Potsdam, Potsdam, Germany, ⁴College of Electronic Information, Wuhan University, Wuhan, China, ⁵Key Laboratory of Earth and Planetary Physics, Institute of Geology and Geophysics, Chinese Academy of Sciences, Beijing, China

Abstract The near-polar orbit satellites of Swarm mission provide a good opportunity to investigate the conjugacy of equatorial plasma irregularities (EPIs) since their trajectories at low latitudes are basically aligned with fixed geographical longitude. However, the Swarm in situ electron density occasionally shows EPIs at only one hemisphere at this longitude. In this study, we provide detailed analysis of such EPI events from the in situ electron densities and onboard global positioning system (GPS) measurements of Swarm low pair satellites, and simultaneous GPS data from two geomagnetically conjugate ground stations at the Africa longitudes. The result indicates that when Swarm in situ electron density sometime shows EPIs at only one hemisphere, the GPS scintillations are still observed from the Swarm onboard receiver and by the two conjugate ground stations. It implies that the EPIs should generally elongate along the geomagnetic flux tube. More than two-year statistic results show that the onset time of scintillation in the northern station is on average 16 and 18 min earlier than that in the southern station for September equinox and December solstice in 2015, while for March equinox in 2016 the onset time of scintillation of northern station is about 11 min later than that of southern station, which indicates the asymmetry features of EPIs along the flux tube. Further analysis of nearly three-year GPS data from two conjugate stations at the Asia longitudes, we find that during solar maximum years the local sunset time plays an important role for causing the difference of onset time of scintillation between two conjugate stations.

1. Introduction

The equatorial plasma irregularities (EPIs), also known as equatorial plasma bubbles, with various scale sizes ranging from centimeters to hundreds of kilometers are generated at the equatorial and low latitudes after sunset, and they are manifested as equatorial spread *F* in ionograms and radar echoes (e.g., Kelley, 2009). After sunset, the plasma density at ionospheric *E* region decays rapidly due to the absence of sunlight; thus, the *E* region conductivity becomes weak. The larger ion-neutral recombination at lower altitude further benefits to generate a steep vertical plasma density gradient toward the topside *F* region, which is opposite to the direction of the gravity. Under the action of Rayleigh-Taylor instabilities, the EPIs are generated at the bottom side of *F* region and raised up to the higher altitudes due to the enhanced $\mathbf{E} \times \mathbf{B}$ drift caused by the prereversal enhancement of eastward electric field around sunset hours; meanwhile, due to large conductivity along the magnetic flux tubes, the small-scale irregularities mainly elongate along the field lines (e.g., Kelley, 1989; Mendillo, 1997). When radio wave signals of global navigation satellite system (GNSS) pass through the irregularities, the signal phase and amplitude will suffer random fluctuations known as ionospheric scintillation (e.g., Crane, 1997), which has the possibility to degrade the performance of GNSS (e.g., Aquino et al., 2005; Luo et al., 2018; Moreno et al., 2011).

The EPIs are assumed to extend along the geomagnetic field lines and sometime can reach above $\pm 20^\circ$ magnetic latitudes (e.g., Balan et al., 2018). This feature has been confirmed by the investigation of simultaneous observations from the ground instruments located at geomagnetically conjugate points in both hemispheres. Otsuka et al. (2002) reported large-scale equatorial *F* region airglow depletions around midnight hours (23:57–01:27 local time (LT)) on 12 November 2001 from two geomagnetically conjugate stations at Sata in Japan (31.0°N, 130.7°E; geomagnetic latitude 24.0°N) and Darwin in Australia longitude (12.4°N,

131.0°E; geomagnetic latitude 22.0°S). The observational results showed that plasma depletion regions with east-west scale sizes of 40–100 km elongate along the geomagnetic field lines in both hemispheres. Focusing on an earlier period of 20:00–21:00 LT, Shiokawa et al. (2004) reported more detailed time evolution of EPIs on 4 April 2002, at geomagnetically conjugate points as Sata and Darwin. To better understand the EPI development along the magnetic flux tubes, a Conjugate Point Equatorial Experiment campaign was established in Brazil in 2002 (Abdu et al., 2009). Combining two conjugate airglow all-sky images as well as the global positioning system (GPS) scintillation data, Sobral et al. (2009) pointed out that a high-degree alignment of the bubbles along the geomagnetic field lines during their development. Recently, the simultaneous observations of zonal drift of equatorial plasma bubbles and the thermospheric neutral winds at geomagnetically conjugate points in the Asian longitudes were reported by Fukushima et al. (2015). They found that under the action of neutral winds the plasma bubbles continuously propagated eastward with velocities of 100–125 m/s and mapped to the conjugate points in two hemispheres. All results mentioned above indicate that the equatorial plasma bubbles are geomagnetically connected at low latitudes.

Due to the effects of EPIs, GNSS in return becomes a powerful tool to investigate EPIs and ionospheric scintillations. At present, the GPS ionospheric scintillation monitor receivers (ISMRS) with the resolution of 50 Hz or even higher have been installed at the Conjugate Point Equatorial Experiment campaign in Brazil, and the corresponding data were also used to study the conjugacy of EPIs (e.g., Abdu et al., 2009). However, ISMRs are not commonly installed at regional or global GNSS networks since such high sampling rate data require substantial memory capabilities and higher costs. Many studies therefore focused on establishing the ionospheric scintillation index based on common GNSS receivers data (1- or 30-s sampling rate) to investigate the ionospheric irregularities (e.g., Juan et al., 2017; Pi et al., 1997). The most common one is the rate of total electron content (TEC) index (ROTI) based on GNSS dual-frequency carrier phase measurements. On the other hand, few studies have shown that the amplitude scintillation index S_4 can also be derived from carrier-to-noise ratio (C/N_0) measurements released by common GNSS receivers (e.g., Juan et al., 2018). Using these indexes, especially derived from common GNSS receivers, to study the conjugacy of EPIs is still very limited. Considering the advantages of high temporal and spatial resolution, GNSS ROTI and S_4 information would further expand the knowledge of generation and evolution processes of EPIs and related scintillation effects.

Except the ground-instrument observation, the space-based database is also widely used to investigate the conjugacy of EPIs. In early stage, the in situ ion density measurements from the atmosphere explorer (AE-E) satellite have been applied to investigate the EPIs aligned along the magnetic flux tube (Weber et al., 1982). After that, the ion density from the Defense Meteorological Satellite Program (DMSP) and the Republic of China Satellite (ROCSAT-1) satellites were used to provide supporting evidence of conjugate phenomena (Martinis & Mendillo, 2007). In addition, the global seasonal/longitudinal distribution of EPIs was also studied based on plasma density measurements from the DMSP, ROCSAT-1, Challenging Minisatellite Payload (CHAMP), and Swarm satellites (e.g., Burke et al., 2004; Kil, Paxton, et al., 2009; Stolle et al., 2006; Su et al., 2006; Wan et al., 2018). From the global map of EPIs, the latitudinal distribution of EPI magnetic signatures is generally symmetrical about the magnetic equator. Moreover, the EPIs from the ground all-sky imager observations also showed that the EPI structures mapped onto two hemispheres agree well with each other as mentioned above (e.g., Fukushima et al., 2015; Shiokawa et al., 2004). But recent studies indicated that the scintillations associated with EPIs were not simultaneously observed by the geomagnetically conjugate GPS receivers (Shume & Mannucci, 2013) and very high frequency radars (De Paula et al., 2010). In addition, the Swarm in situ electron density profiles occasionally show quite different structures of EPIs at conjugate points of two hemispheres. For example, on 20 October 2014, the electron density measured by Swarm C (around $\sim 3.8^\circ$ geographical longitude) showed strong depletions in the northern hemisphere (NH), while no obvious depletions were seen in the southern hemisphere (SH; Xiong et al., 2018). Compared to the low Earth orbital (LEO) satellites with low-inclination orbits, the satellites with polar orbits, like the CHAMP satellite as well as the Swarm mission, are more suitable for investigating the conjugacy of EPIs since their trajectories at low and middle latitudes are basically aligned with fixed geographical longitude. It also should be mentioned that the Swarm in situ electron density only provides point measurements along its orbit, which can be considered as very “local” measurements. For the ground-based GNSS receivers, the signals received from different GNSS satellites usually propagate from different directions, so it has a larger field of view for monitoring the ionospheric irregularities. In this study, we

therefore use the combined data from space-based Swarm satellites and the ground-based GPS receivers to analyze the conjugacy and asymmetry of EPIs along the magnetic flux tube. In particular, we first present detailed analysis of EPIs from the in situ electron density measurements of the lower pairs of Swarm satellites. Then the simultaneous GPS scintillation indexes (ROTI and S_4) derived from two conjugate ground stations at the Africa longitudes are also used to investigate the EPIs. In addition, the onset time of scintillation (OTS) at the two conjugate stations is also detailed analyzed in this study.

2. Data and Methodology

2.1. The Swarm Satellites

Swarm is the fifth European Space Agency's Earth Explorer mission and consists of three satellites of near-polar orbits (Friis-Christensen et al., 2008). They were launched on 22 November 2013 with initial altitude of about 500 km. The lower pair, Swarm A and C, is flying side by side (1.4° separation in longitude) at an altitude of 450 km, while swarm B flies at an altitude of 530 km. Two Langmuir probes onboard of each Swarm satellite provide the electron density and temperature along the satellite track. The detailed data resolution, calibration, and validation of Swarm plasma density are summarized in Knudsen et al. (2017) and Lomidze et al. (2018). Dual-frequency GPS receivers are equipped on onboard the Swarm satellites for providing the GPS data, including the pseudorange, carrier-phase, and C/N_0 measurements (van den Ijssel et al., 2016). In this study, we used the Swarm A and C in situ electron density (2-Hz sampling rate) and GPS carrier-phase measurements (1-Hz sampling rate) provided by level 1b product (Swarm document, 2018).

2.2. Ground-Based GPS Measurements From Geomagnetically Conjugate Points

The GPS carrier-phase and C/N_0 measurements collected at two geomagnetically conjugate stations, MAS1 (27.8°N , 15.6°W ; geomagnetic latitude 19.8°N) and ASCG (7.9°S , 14.3°W ; geomagnetic latitude 19.2°S) located at the Atlantic islands (see Figure 1) are also used. The two stations are selected since the axis of them is near perpendicular to the magnetic equator. The northern station MAS1 is equipped with Septentrio PolaRx4 receiver and the data are available since September of 2012, while the southern station ASCG is equipped with Trimble NetR9 receiver and the data are available since September of 2015. Considering the data coverage of two stations, more than two years data from 24 September 2015 to 31 December 2017 are used in this study. To reduce the effects of non-EPIs related tracking error such as multipath, only the GPS data observed above 30° elevation angle are considered (Jiao et al., 2013; Zhang et al., 2017).

2.3. Ionospheric Scintillation Indexes

Ionospheric scintillation indexes, including the phase and amplitude scintillation index σ_ϕ and S_4 , are generally obtained from dedicated GNSS receivers, that is, ISMRs, with high data sampling rates of typically 50 Hz. However, the ISMRs are not commonly installed in the network-based GPS monitoring system. Pi et al. (1997) proposed an alternative index called ROTI based on a lower data sampling rates of 30 or 1 s collected by the common GPS receivers. The ROTI is defined as the standard deviation of rate of TEC with a sliding window for each 5-min interval:

$$\text{ROTI} = \sqrt{\langle \text{ROT}^2 \rangle - \langle \text{ROT} \rangle^2} \quad (1)$$

The ROT at epoch (k) can be calculated by the differencing TEC for each 30- or 1-s interval

$$\text{ROT} = \frac{\text{TEC}(k) - \text{TEC}(k-1)}{\Delta t} \quad (2)$$

where TEC, in a unit of TECU ($1 \text{ TECU} = 10^{16} \text{ el/m}^2$), at the epoch (k) can be estimated with high precision from a geometric-free combination of the carrier phase measurements.

For the space-based GPS data, we apply a threshold of ROTI larger than 5 TECU/min together with a condition of multiplex detection algorithm for identifying the EPIs, as introduced by Zakharenkova et al. (2016). For the ground-based GPS data, we apply a threshold of ROTI larger than 2 TECU/min, which is similar to Yang and Liu (2017), to identify the scintillation caused by EPIs. Note that the threshold of ground-based ROTI is smaller than that of space-based ROTI. The reason is that compared to the ground-

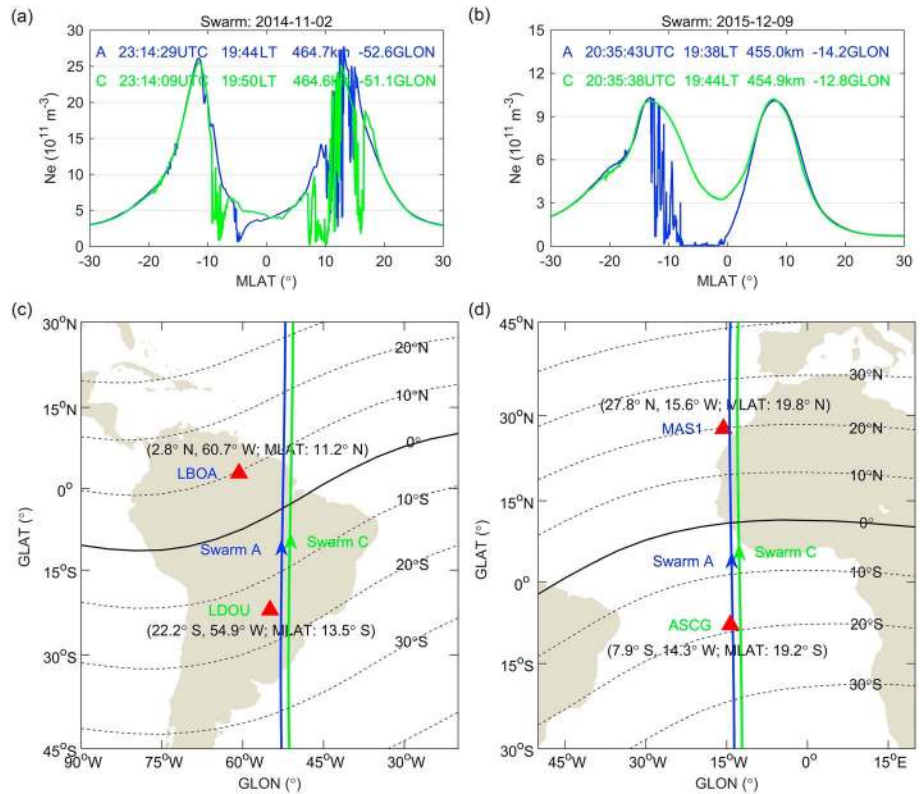


Figure 1. (a) Time series of in situ electron density measurements from Swarm A (blue) and C (green) when they pass through two conjugate stations LBOA and LDOU located in the South America longitudes. (b) Same as in (a) but for stations MAS1 and ASCG located in the Africa longitudes. The geographical location of those stations is shown in Figures 1c and 1d, respectively.

based ROTI, the latter one shows a mixing of moving ionospheric structures/irregularities and rather stationary ionospheric gradients (Zakharenkova et al., 2016).

Except the ROTI index, we also show an alternative amplitude index S_4 derived from GPS C/N_0 measurements with 1-s interval in this study. The availability of this index was confirmed by Juan et al. (2018). The calculation of the S_4 can be expressed as (van Dierendonck et al., 1993)

$$S_4 = \sqrt{\frac{\langle (\text{SI}_{\text{detrended}}^{S/N_0})^2 \rangle - \langle \text{SI}_{\text{detrended}}^{S/N_0} \rangle^2}{\langle \text{SI}_{\text{detrended}}^{S/N_0} \rangle^2}} \quad (3)$$

where the $\text{SI}_{\text{detrended}}^{S/N_0}$ represents the detrended signal intensity (SI) based on signal-to-noise ratio (S/N_0). The $\text{SI}_{\text{detrended}}^{S/N_0}$ and S/N_0 can be calculated as

$$\text{SI}_{\text{detrended}}^{S/N_0} = \frac{(S/N_0)_k}{\sum_{i=1}^{60 \times f_s} \frac{(S/N_0)_{k-i}}{60 \times f_s}} \quad (4)$$

$$S/N_0 = 10^{0.1(C/N_0)} \quad (5)$$

where the f_s represents the sampling interval 1 s in this study.

Similar to the index S_4 released by ISMRs, the threshold of S_4 derived from 1-s C/N_0 measurement outputted by the common receivers is also defined as 0.2.

3. Analysis and Results

3.1. EPIs Observed by the Swarm Satellites When Flying Over Longitudes of Different Magnetic Declination

In Figure 1, two examples of electron density profiles of EPIs observed by Swarm A and C when they fly at different longitudes are shown. The coordinated universal time (UTC), LT, altitude, and geographic longitude when the satellites pass over the geographic equator are listed at the top side. The 1.4° longitudinal separation between Swarm A and C corresponds to about 6-min difference in LT at equatorial and low latitudinal regions. The first example as shown in Figure 1a is observed on 2 November 2014, and the electron densities measured by Swarm A and C both show clear depletions in the NH (7° – 17° magnetic latitude (MLAT)), while no significant depletions above -10° MLAT are observed in the SH. Note that the magnetic declination is about -15° around -52° E longitude, so in this example the Swarm satellites cut through different magnetic flux tube in the two hemispheres. That is probably why both Swarm satellites observed different structures of EPIs at the two hemispheres.

The second example as shown in Figure 1b is observed on 9 December 2015 when Swarm A and C fly around -15° E longitude where the magnetic declination is close to zero (see Figure 1d), which means that the Swarm orbits are almost aligned with the flux tube in the two hemispheres. However, small-scale plasma depletions are only seen in the SH but not in the NH. Interestingly, the depletions at the SH are only observed by Swarm A, which is possibly due to the relatively thin longitudinal extension of EPIs as reported by Xiong et al. (2016, 2018). The second example presented here also indicates that the small-scale plasma depletions associated with EPIs may not be equally distributed along the geomagnetic flux tube. In the following, we provide more detailed analysis from two examples of simultaneous observations from Swarm and ground-based GPS measurements.

3.2. EPIs Observed by the Swarm Satellites in Both the NH and SH

On the night of 24 November 2015, the Swarm satellites flew over the conjugate stations MAS1 (NH) and ASCG (SH). Among them, Swarm A flew over ASCG and MAS1 at 21:42:31 and 21:51:48 UTC, corresponding to 20:45:19 and 20:49:24 LT, respectively, and Swarm C was 1.4° eastward of Swarm A. Figure 2a shows the time series of in situ electron density measurements from the two satellites. Since the trajectory of Swarm A is closer to the ground stations, the UTC, geographic latitude, geographic longitude, MLAT, and magnetic local time from the orbital arc of Swarm A are listed at the bottom of the figure. The density depletions along the orbital arcs of two satellites are observed in both the NH and SH, but show quite different structures. Compared with the SH, the smaller depletions are shown in the NH for both satellites. In the southern EIA region, large depletions from -17.4° to -5.0° MLAT are observed by both satellites, while the depletions between -23.6° and -17.4° MLAT are only observed by Swarm C.

Figures 2b and 2c present the ROTI information derived from the carrier-phase measurements of GPS receiver onboard Swarm A and C, respectively. The trajectories of GPS satellite with different pseudo-random noise are represented by the ionospheric pierce points mapped onto an altitude of 455 km. The blue and green dashed lines represent the trajectories of Swarm A and C, and only the GPS trajectories with space-based ROTI larger than 5 TECU/min during the considered period are depicted. As shown in Figures 2b and 2c, in the SH the ROTIs from Swarm A show large values (>5 TECU/min) between -20.0° and -10.0° MLAT, but ROTI from Swarm C with values larger than 5 TECU/min are found extended to -25.0° MLAT. From Figure 2a, we note that in the SH the EPIs observed by Swarm A and C in situ electron density reach as high as -17.4° MLAT and -23.6° MLAT, respectively, which agrees well with the ROTI observations. In the NH, the ROTIs of G18, G20, and G24 tracked by Swarm A present larger values at the regions between 4.0° and 20.0° MLAT.

Figure 3 presents the time series of ROTI and S_4 for the GPS satellites observed at conjugate stations MAS1 (NH) and ASCG (SH) during the nighttime period of 16:00–24:00 LT on 24 November 2015. From Figure 3, it can be seen that no significant fluctuations are seen from the time series of ROTI and S_4 between 16:00 and 19:10 LT, while during 19:30–23:00 LT both indexes fluctuate significantly with respect to the enhanced scintillation activity. Around 21:30 LT, the maximum of ROTI and S_4 can reach 14 TECU/min and 1.3, respectively. Such intense scintillation should be caused by the strong EPIs, which has been proved by the in situ electron density measurements of Swarm A and C (see Figure 2a). We note that the S_4 index with values

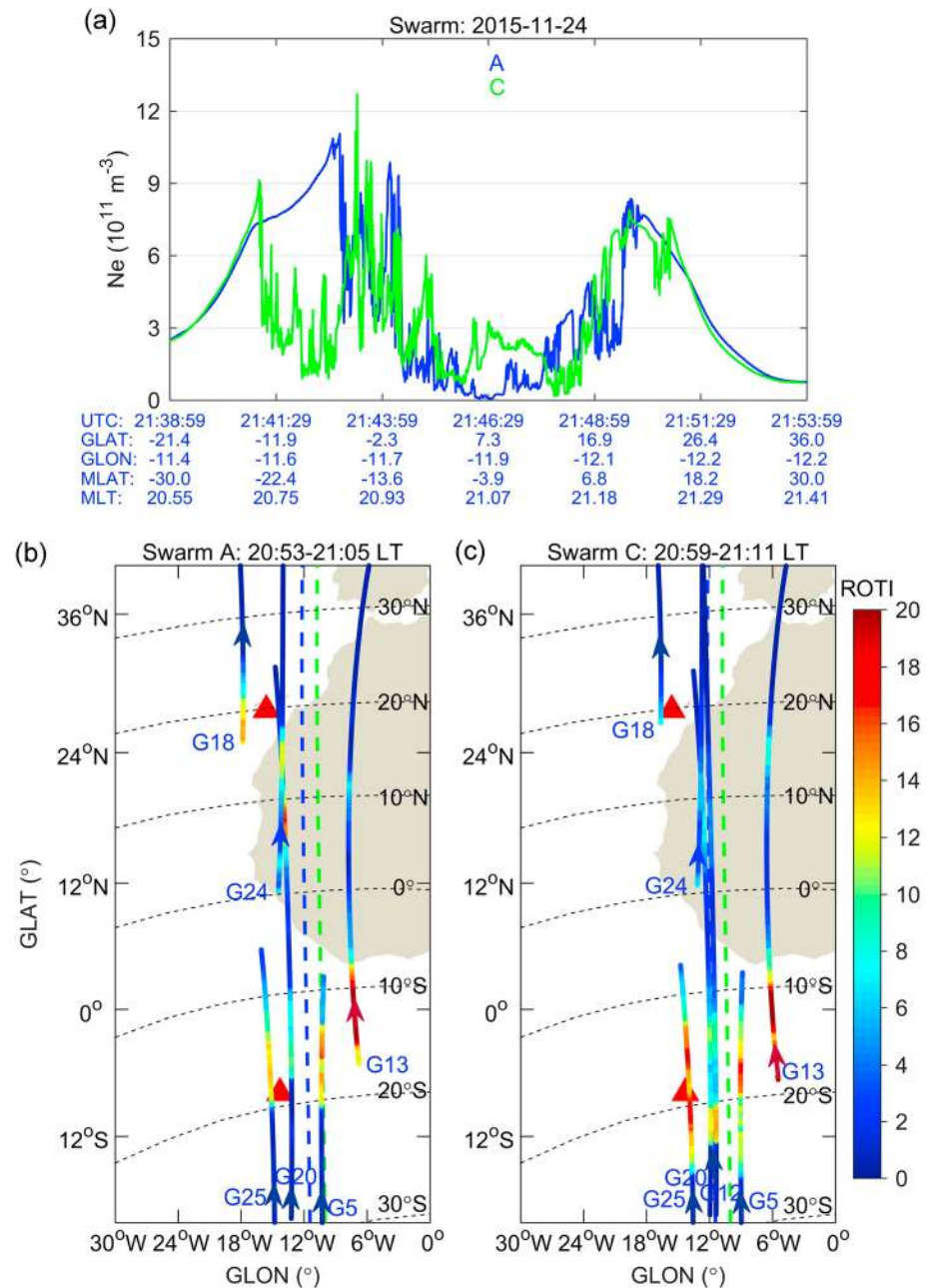


Figure 2. (a) Time series of in situ electron density measurements from Swarm A (blue) and C (green) when they pass through the two conjugate stations MAS1 (NH) and ASCG (SH) on 24 November 2015. (b) The ROTI along the trajectories of GPS satellites tracked by the spaceborne receiver of Swarm A. (c) Same as in (b) but for Swarm C.

larger than 0.2 for the station ASCG are also seen during nonscintillation period. These anomalous values can be caused by many factors, such as the random noise since the strategies of noise processing are different for various types of GPS receivers, but the anomalous values of S_4 seldom exceed the value of 0.5 (e.g., Luo et al., 2018).

In addition to the temporal variations, the spatial distributions of the corresponding ROTI and S_4 for each affected GPS satellites from the two ground stations are shown in Figure 4. Note that only the GPS trajectories with ground-based ROTI larger than 2 TECU/min during the considered period are depicted in the figure. As shown in Figure 2, stronger depletions of EPIs are found at the EIA crest regions. Therefore, larger values of ROTI and S_4 are seen located at the southward for the station MAS1 and the northward for the

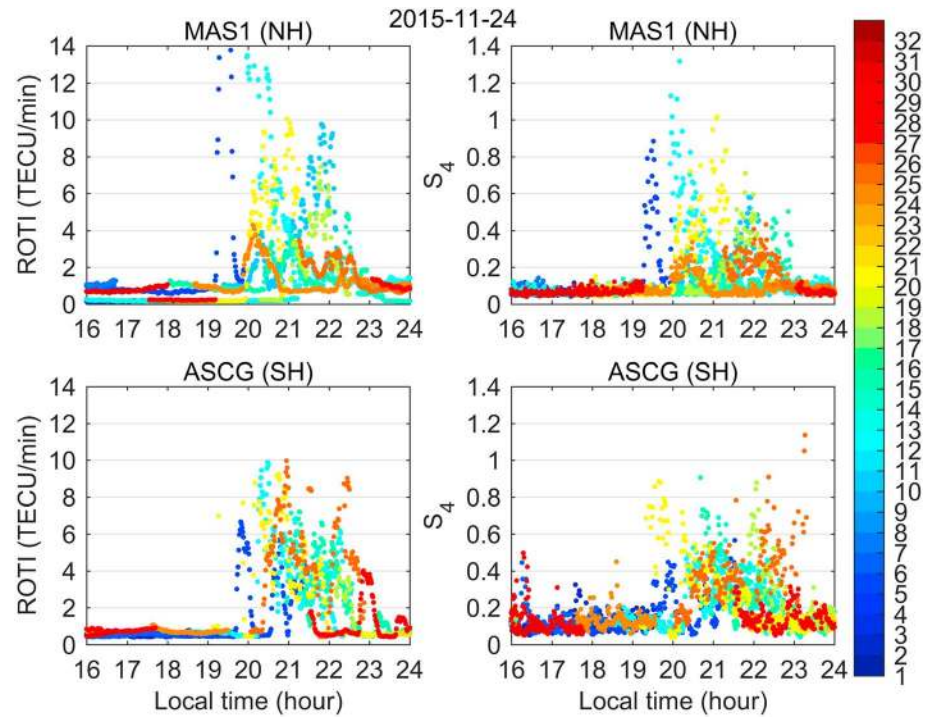


Figure 3. Time series of ROTI and S_4 of GPS satellites observed at two conjugate stations MAS1 (NH) and ASCG (SH) on 24 November 2015. Each GPS satellite uses one color to represent its ROTI and S_4 , as indicated in the color bar.

station ASCG as these two stations are located at the poleward of EIA crests. Comparing the Swarm in situ and ground GPS measurements, we can see that when Swarm encounters EPIs at two hemispheres, scintillation are also observed from the two conjugate stations. The above results support that the EPIs should extend along the geomagnetic flux tube.

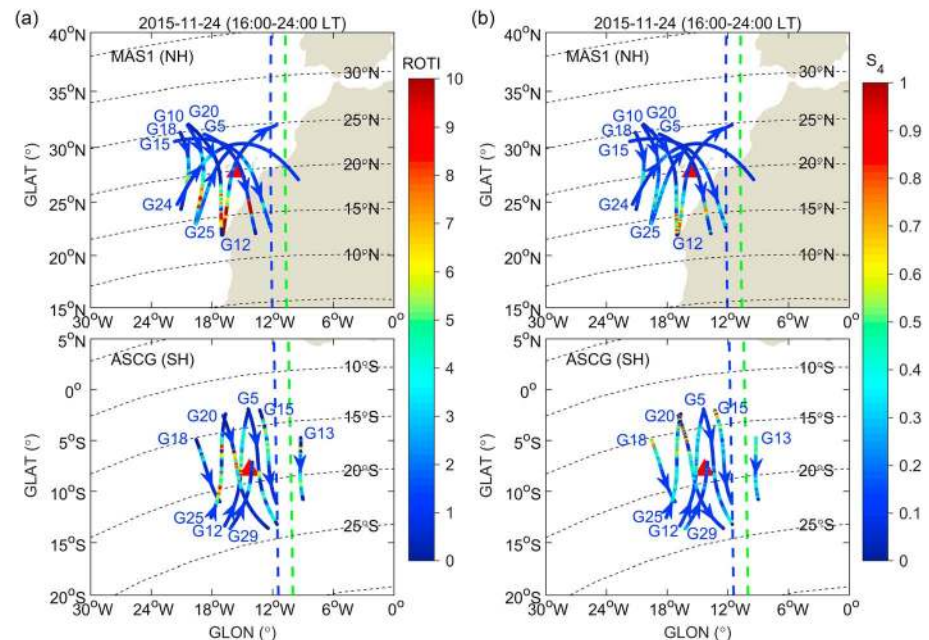


Figure 4. The ROTI and S_4 along the trajectories of GPS satellites tracked by the two conjugate stations MAS1 (NH) and ASCG (SH) during 16:00–24:00 LT on 24 November 2015.

3.3. EPIs Observed by the Swarm Only in the SH

Figure 5 presents another example on 9 December 2015, with EPIs observed only in the SH from the in situ electron density of Swarm satellites. Swarm A flew over the conjugate stations MAS1 (NH) and ASCG (SH) at 20:30:53 and 20:40:10 UTC, corresponding to 19:33:41 and 19:37:46 LT, respectively, and Swarm C was 1.4° eastward of Swarm A. As shown in Figure 5a, the in situ electron density measurements from Swarm A (blue) show clear depletions at the region between -14° and -7.0° MLAT, while no depletions are seen from Swarm C (green). In the NH, neither satellites observe depletions. An interesting feature seen here is that from -8° MLAT to magnetic equator (see the top-right panel in Figure 5a), the electron density measured by Swarm A is extensively lower ($\sim 4 \times 10^{11} \text{ m}^{-3}$) than that measured by Swarm C, although no small-scale depletions are observed there.

From Figure 5b, larger ROTI values derived from Swarm A are distributed at the region between -17° and -8° MLAT, which is consistent with the depletions of in situ electron density measured by Swarm A. At this region, the GPS satellite with pseudo-random noise of G5, G13, and G25 show larger ROTI values (~ 20 TECU/min) than those of G12 and G20 (~ 8 TECU/min). This implies that the depletion magnitude of EPIs is stronger in both eastern and western sides of ASCG. From Figure 5c, we can see that G5 and G25 tracked by Swarm C show smaller ROTI values in the SH compared to the same GPS satellites tracked by Swarm A. That is consistent with no obvious depletions observed from the in situ electron density measurements of Swarm C (see Figure 5a). In addition, there are only three satellites trajectories (G5, G18, and G25) with ROTI larger than 5 TECU/min, which also agrees with that of no depletions observed in the in situ electron density of Swarm C. It is worth to mention that the ROTI of G25 shows values larger than 5 TECU/min between -17° and -12° MLAT, as the trajectory of G25 is located at the westside for both Swarm A and C, which also means the radio wave signal of G25 received by Swarm C has to propagate through regions of EPIs as detected by Swarm A. But for G5 located on the eastside of Swarm C, the radio wave signal received by Swarm C does not propagate through regions of EPIs as detected by Swarm A; therefore, no obvious fluctuations are seen from the corresponding ROTI values. The above analyses show nice consistency between the Swarm in situ electron density and onboard GPS measurements.

The time series of ROTI and S_4 for the GPS satellites observed at stations MAS1 (NH) and ASCG (SH) during the period of 16:00–24:00 LT on 9 December 2015 are shown in Figure 6. It can be clearly found that although the EPI is only detected in SH by Swarm A, the scintillations are still observed by ground-based stations of both sides. This difference is possibly due to the fact that the Swarm only provides point measurements of electron density along its trajectory, while the GPS signals received by either the spaceborne or the ground-based receivers can be affected by plasma irregularities existing along the signal path. The other possible reason could be related to the time delay when Swarm constellation passes through two conjugate stations. For example, assuming a typical eastward drift velocity of EPIs on the order of 100–200 m/s (Kintner & Ledvina, 2004; Valladares et al., 2002), with time delay of ~ 10 min when Swarm satellite flies from the southern to northern EIA crest, the EPI can be drifted eastward by about 60–120 km. In addition, the scintillation of the ground GPS receiver of this case is much lower than that of the first case, and only three satellites experience scintillation as shown in Figure 6. From the figure, we can also see a hemispheric asymmetry in scintillation on 9 December 2015.

The spatial distributions of their ROTI and S_4 are shown in Figure 7. As we can see that the ionospheric pierce points with scintillation occurrence are distributed in the south of MAS1 and the northeast of ASCG. For the southern station ASCG, the scintillation is stronger at eastside than that at the westside of station. In this example, even though the Swarm in situ electron density shows small-scale depletions at only one hemisphere, scintillation from both spaceborne and ground receivers are observed at two hemispheres. It also indicates that the EPIs do exist in both hemispheres, but the small-scale structures possibly do not equally distribute along flux tube.

3.4. OTS From the Two Conjugate Stations

Three-month variations of ROTI derived from the two conjugate stations from 24 September to 31 December 2015 are shown in Figure 8. The absent of ROTI values on 25 December 2015 (day of year 359) is due to the lack of GPS measurements of MAS1 station on that day. Generally, the time variation of ROTI derived from the northern station MAS1 agree well with that derived from the southern station ASCG, and the amplitudes

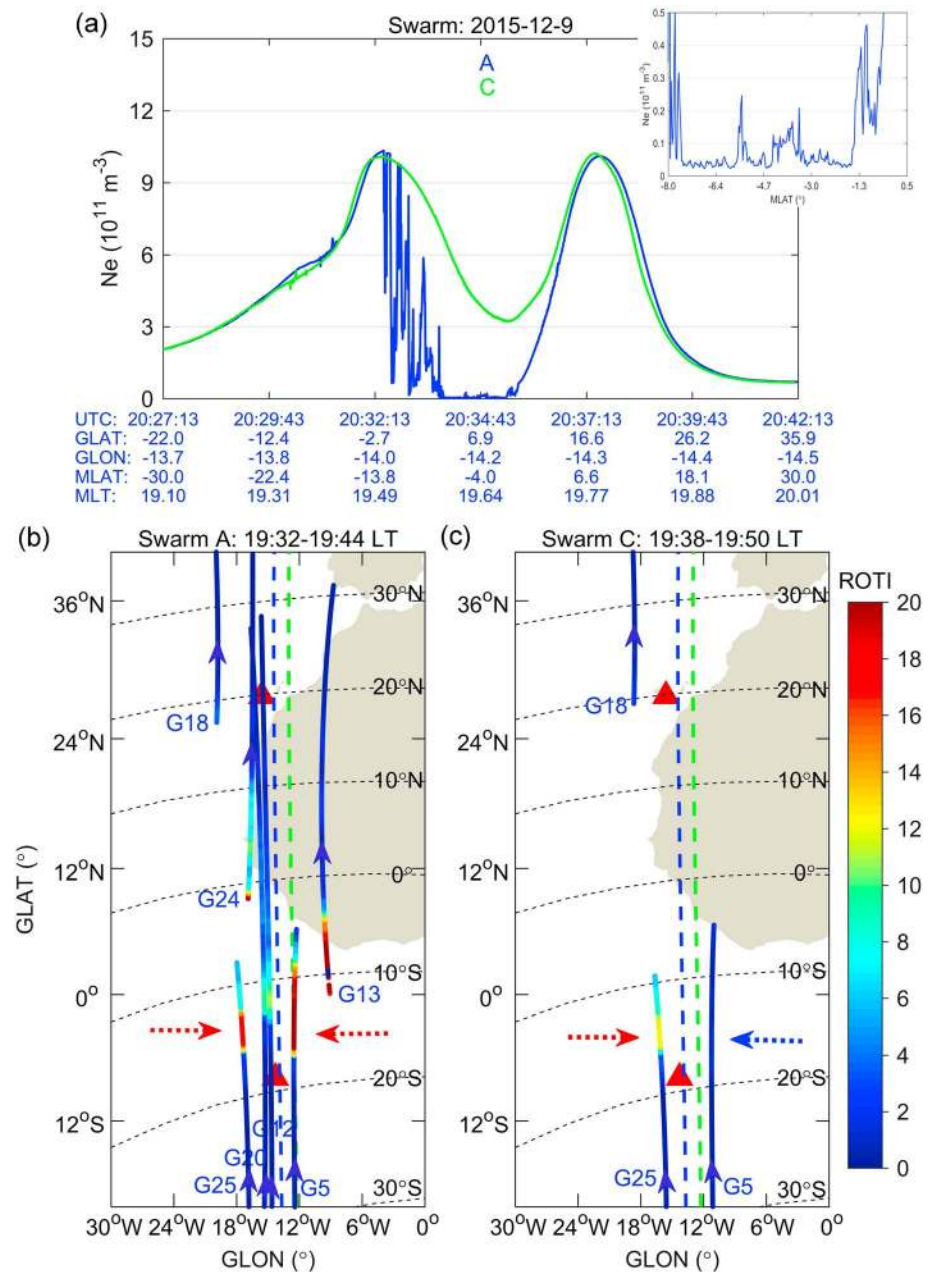


Figure 5. (a) Time series of in situ electron density measurements from Swarm A (blue) and C (green) when they pass through two conjugate stations MAS1 (NH) and ASCG (SH) on 9 December 2015. The time series of in situ electron density from Swarm A from -8.0° to 0.5° MLAT are amplified in the top right of Figure 5a. (b) The ROTI along the trajectories of GPS satellites tracked by the spaceborne receiver of Swarm A. (c) Same as in (b) but for Swarm C.

of ROTI for both stations are comparable on the whole. It means that for most cases the scintillations occur in both stations, suggesting that the EPIs are extended along the geomagnetic flux tube. Interestingly, some special cases, such as scintillation occurred in only one station, are also observed. For example, on 2 December 2015 (day of year 336) as shown in Figure 9, no ROTI values exceed 2.0 TECU/min for station MAS1, but for the station ASCG, ROTI derived from different GPS satellites with values exceeding 2.0 TECU/min (largest values reaching as high as 10 TECU/min) persists as long as for 2 hr (21:00–23:00 LT). For the amplitude scintillation, an obvious variation of S_4 can be seen during the nighttime of 21:30–23:00 LT and the values can reach around 1.0. Compared to ROTI index, the time series of S_4 index show more significant fluctuation. Several studies showed that at low-latitude regions the amplitude

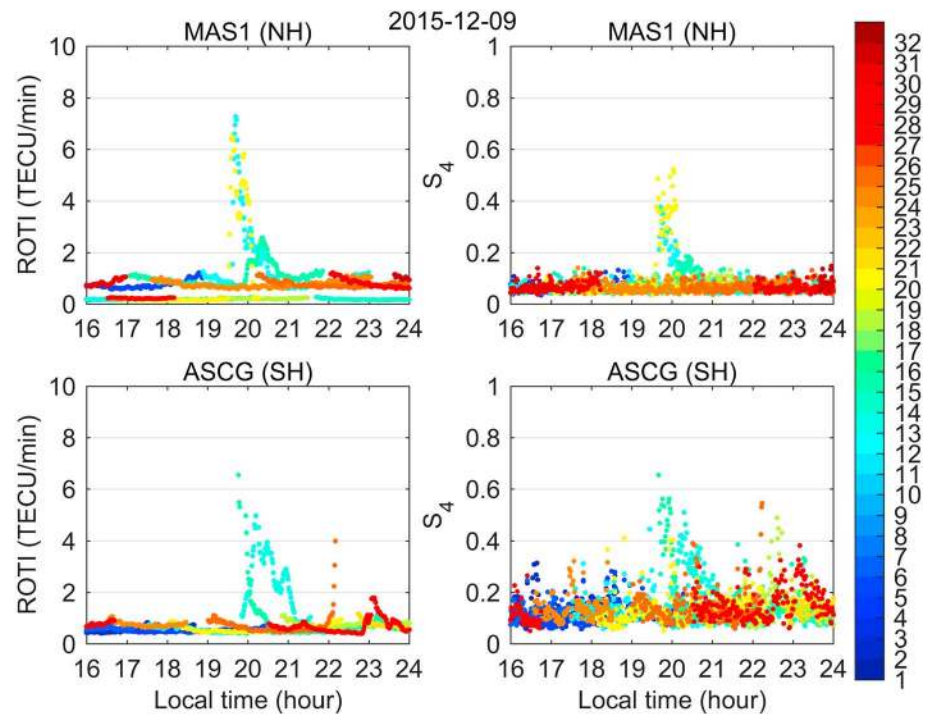


Figure 6. Time series of ROTI and S_4 for GPS satellites observed at two conjugate stations MAS1 (NH) and ASCG (SH) on 9 December 2015. Each GPS satellite uses one color to represent its ROTI and S_4 , as indicated in the color bar.

scintillation occurrence is generally more frequent than that of phase scintillation (e.g., Gwal et al., 2006; Spogli et al., 2013).

We further compare the OTS for the two stations, and the result is shown in Figure 10. The blue and green points in the upper two panels represent the OTS of MAS1 and ASCG stations, respectively, and the black dashed lines show the local sunset time at 300-km altitude. The red points in the third panel represent the

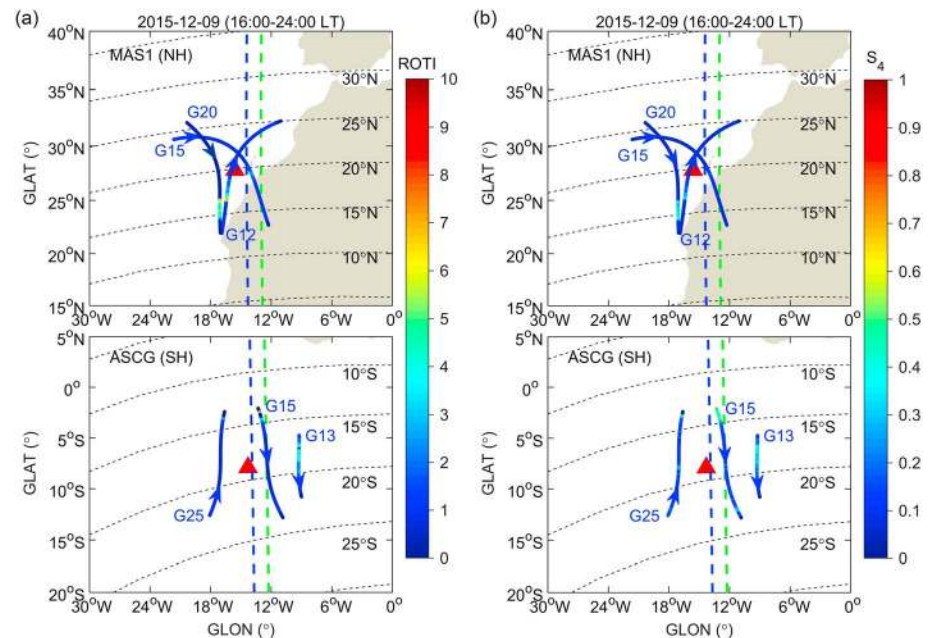


Figure 7. The ROTI and S_4 along the trajectories of GPS satellites tracked by the two conjugate stations MAS1 (NH) and ASCG (SH) during 16:00–24:00 LT on 9 December 2015.

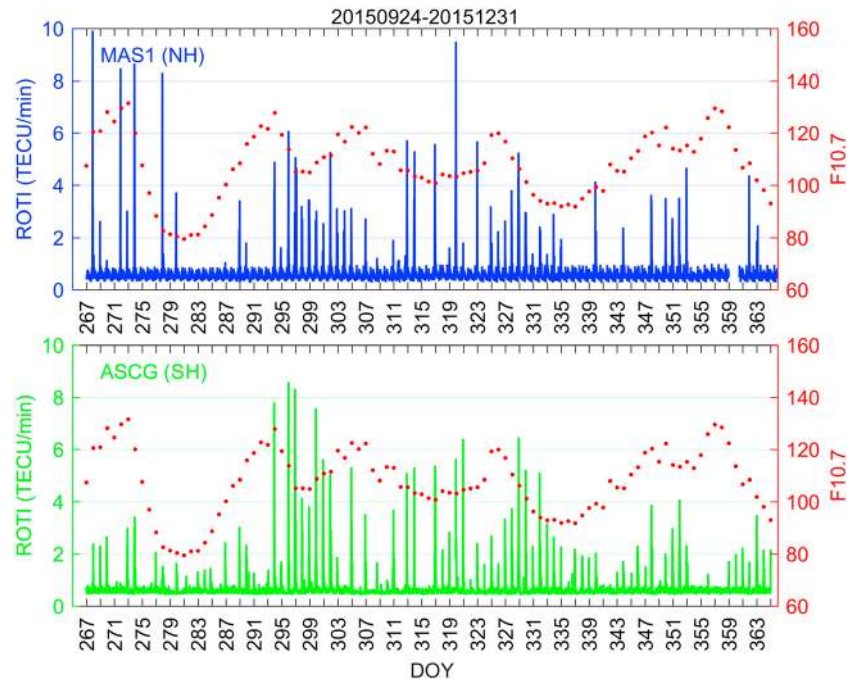


Figure 8. Daily variations of ROTI for the two conjugate stations MAS1 (NH) and ASCG (SH) from 24 September to 31 December 2015. The red points represent the variation of solar flux $F_{10.7}$ index.

time difference of OTS between MAS1 and ASCG stations. In addition, the detailed statistics of OTS events in two hemispheres, their time difference, and the corresponding sunset time difference for different seasons are given in Table 1. The equinoxes include March, April, September, and October. The December and June solstice include months from November to February, and from May to August, respectively. From

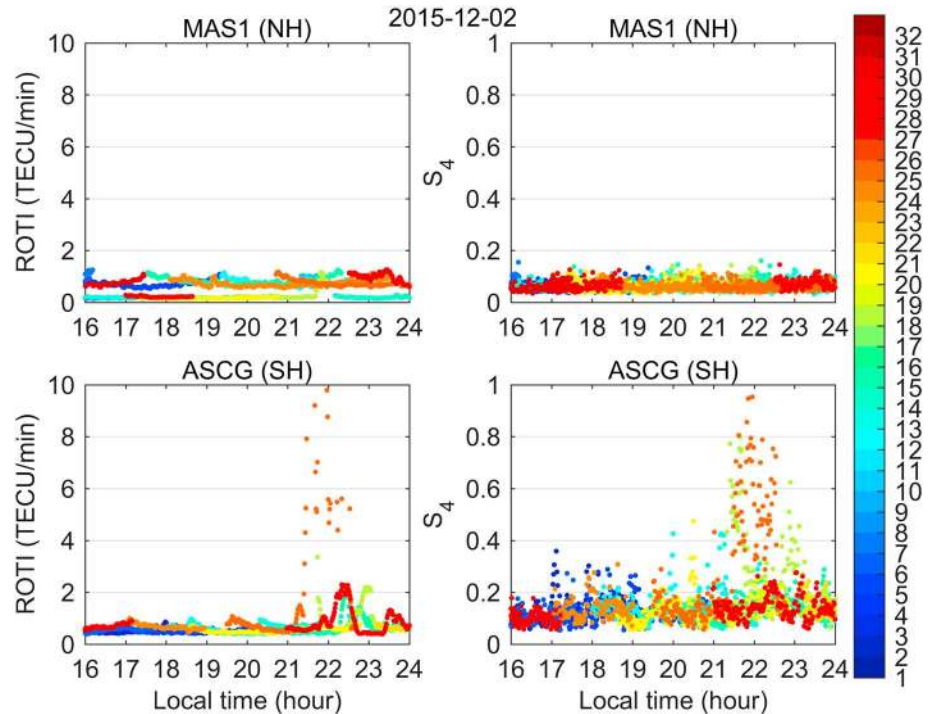


Figure 9. Time series of ROTI and S_4 for GPS satellites observed at the two conjugate stations MAS1 (NH) and ASCG (SH) on 2 December 2015.

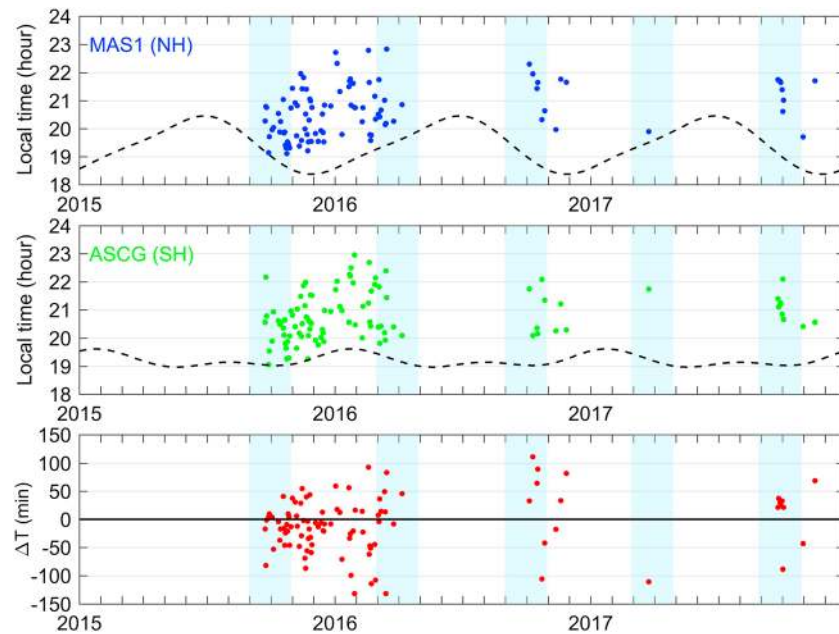


Figure 10. The OTS of MAS1 (NH) and ASCG (SH) as well as their difference (ΔT) from 24 September 2015 to 31 December 2017. The black dashed lines represent the local sunset time and the equinoctial (March–April, September–October) months are highlighted in blue.

the figure, the daily variations of OTS for the two conjugate stations are comparable during the period from 25 September 2015 to 31 December 2017. The results further indicate that for most situations the time of EPIs appearance is quite close, suggesting that they are distributed along the geomagnetic flux tube. Yokoyama et al. (2004) showed that the EPIs exclusively initiated near sunset. If we assume they later extend with equally speed along the magnetic flux tube into low latitudes at two hemispheres, the two stations at conjugate nodes should observed EPIs at almost the same time. However, the detailed OTS statistics for different seasons shown in Table 1 indicate an obvious asymmetry of OTS in two conjugate stations. For seasons of September equinox and December solstice in 2015, the scintillation occurred in the NH is earlier (~16 and ~18 min) than that occurred in the SH, and the corresponding local sunset time at 300-km altitude for MAS1 (NH) is also earlier (~12 and ~45 min) than that for ASCG (SH). For season of March equinox in 2016, we can see that the scintillation occurred in the NH is ~11 min later than that occurred in the SH, which also agrees with the corresponding later sunset time of ~21 min in the NH. However, this correspondence is not found in other seasons of 2016 and 2017. Note that very few OTS events occurred during the two solar minimum years.

To further check the relationship between OTS and local sunset time as well as local seasons, nearly three-year GPS measurements from another two geomagnetically conjugate stations, SANY and BAKO, in the Asia region are further analyzed. The northern station SANY (18.3°N, 109.6°E; geomagnetic 11.5°N,

Table 1

Statistics of the Number of OTS Appeared Earlier in NH, SH, the Time Difference (ΔT) of OTS, and the Corresponding Sunset Time Difference in Different Seasons

Year	Season	NH (Events)	SH (Events)	ΔT OTS (min)	ΔT Sunset (min)
2015	Equinox (September–October)	6	15	−15.9	−12.1
	Solstice (December)	15	33	−18.5	−45.3
2016	Equinox (March–April)	7	3	10.6	21.0
	Solstice (June)	0	0	—	68.3
	Equinox (September–October)	4	2	25.0	−0.6
	Solstice (December)	2	1	32.5	−45.5
2017	Equinox (March–April)	0	1	−110.7	20.7
	Solstice (June)	0	0	—	68.3
	Equinox (September–October)	6	1	11.2	−0.3

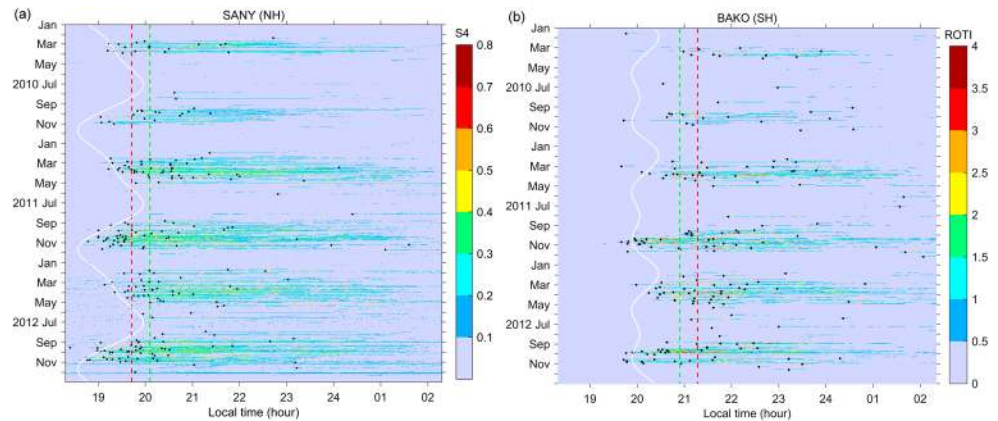


Figure 11. The OTS and its variations during the period of 2010–2012 for the (a) northern station SANY and (b) southern station BAKO. The white curves represent the local sunset time. The red and green vertical dashed lines depict the mean OTS during the autumn and spring months of 2011–2012, respectively. Note that Figure 11a is modified after Liu et al. (2015).

178.4°W) is installed with the ISMR of GSV4004A type and the southern station BAKO (6.5°S, 106.9°E; geomagnetic 15.7°S, 178.7°W) is installed with the common receiver of Leica GRX1200 type. Figure 11 presents the nighttime scintillation during the period of 2010–2012. It should be mentioned that the Figure 11a is modified after Liu et al. (2015). The modifications include the change of background color (blue to gray) and the remove of y axis labeling. The data sampling interval of BAKO is 30 s, so we choose the ROTI to represent the magnitude of scintillation. The black points represent the OTS on a given day. The white curves depict the local sunset time at 300-km altitude. The red and green vertical dashed lines show the mean OTS during the autumn and spring months of 2011–2012. From Figure 11, we can clearly see that the OTS of SANY is earlier than that of BAKO, further suggesting that there is an obvious asymmetry of EPIs along the flux tube. Interestingly, during the solar minimum year of 2010, the OTS in March equinox and September equinox are generally comparable regardless of SANY (NH) or BAKO (SH). That means the OTS has no clear correlation with local sunset time during the solar minimum years, which is also consistent with the observations of MAS1 and ASCG in 2016 and 2017 (see Figure 10 and Table 1). For the relative solar maximum year of 2011 and 2012, the mean sunset time of SANY (NH) during September equinox is about 24 min earlier than that in March equinox, and the OTS at SANY is about 25 min earlier in September equinox than in March equinox. It is also true for the southern station BAKO with about 18 min of sunset and about 23 min of OTS earlier in September equinox. From the above analysis, we can conclude that rather than the local season, the local sunset time is more important for causing the difference of OTS between two conjugate stations.

4. Discussion

Equatorial plasma irregularities are accepted to be generated at low latitudes around the magnetic equator through the generalized Rayleigh-Taylor instability mechanism (e.g., Kelley, 2009). Due to the unstable density perturbations of rapidly rising *F* layer, the large depleted density irregularities can expand along the magnetic field lines to *F* region heights over latitudes off the equator (e.g., Abdu et al., 2009; De Paula et al., 2010). Several studies have shown that the depleted structures of EPIs mapped onto the two hemispheres match closely with each other in the all-sky imager observations (e.g., Fukushima et al., 2015; Otsuka et al., 2002), even for the small-scale structures of less than 50 km (Shiokawa et al., 2004). This study presented two typical examples of EPIs (Figures 2a and 5a) showing different structures observed by the Swarm lower pair satellites, suggesting that the finer structures of EPIs are possibly not equally distributed along the flux tube.

Under the influence of zonal neutral winds, ionospheric conductivity, and plasma zonal drift, the structures of EPIs observed by all-sky airglow imagers sometime show quite different shapes, such as the inverted “C” shell; C shell; or even “Y,” “I,” or “S” shapes, when they are in the developing stage (e.g., Huba et al., 2009; Kil, Heelis, et al., 2009; Wu et al., 2017). Huba et al. (2009) pointed out that the formation of the C shell

structure can be explained by the creation of polarization electric field inside the plasma depleted region or by the zonal shear flow of the ionosphere. For the *Y*-shaped structures, Wu et al. (2017) showed that because the changing of internal polarization electric field, the zonal drift velocity of the east branch was greater than that of the west one. They also pointed out that the *S*-shaped structures of EPIs were possibly associated with the different zonal velocities of EPIs at different latitudes during the EPIs developing process. Therefore, the changes of shapes of EPIs often relate to the motion of ionospheric background plasma, ionospheric conductivity, and zonal neutral winds, thus resulting in the quite different profiles of Swarm in situ electron density (see Figures 2a and 5a). Under the assumption of the increases of eastward plasma drift and zonal neutral wind with decreasing latitudes, it will cause the depletion region drifting faster at latitude further away from the dip equator and generate an eastward tilted structure of EPIs (*C* shell structure). That is why the electron density measured by Swarm C showed earlier than that of Swarm A in SH, and the depleted duration of Swarm C is longer than that of Swarm A in NH (see Figure 2a). On the other hand, Figure 5a shows that in SH the large depletions were observed by Swarm A, while no depletion was observed by Swarm C. If the latitude of zonal drift velocities were basically aligned with the geomagnetic meridian before 20:00 LT in Figure 5a, the EPIs could show an *I* shape. With this assumption, it means that the in situ density depletions between -14° and -7.0° MLAT of Swarm A corresponded to such an *I* shape of EPI with a thin longitudinal extension, and it was not encountered by the trajectory of Swarm C. This hypothesis can also be inferred from the *I* shape of EPI in Figure 4 and the variations of the zonal velocities of that EPI before 21:00 LT in Figure 5 of Wu et al. (2017) and the thin EPIs with longitudinal extension of 20–30 km in Figure 4 of Xiong et al. (2018).

The in situ measurements from Swarm satellites only reflect the plasma variations along the satellite track and there is a time delay (~ 10 min) when Swarm constellation passes through two conjugate stations; therefore, it is hard to analyze the symmetry of EPIs in the flux tube. Based on ground-based GPS data, the ionospheric scintillations shown in Figures 3, 4, 6, 7, and 8 clearly suggest that the EPIs should generally elongate along the geomagnetic flux tube, but still an asymmetry of OTS at two hemispheres can be seen in Figure 10. The comprehensive statistics shown in Figure 11 further indicate that the asymmetry of EPIs along the flux tube. This asymmetrical feature of scintillations between two conjugate points has been also pointed out by De Paula et al. (2010) based on GPS S_4 data collected at the Conjugate Point Equatorial Experiment campaign in Brazil. A question may arise that the GPS medium Earth orbit (MEO) satellites with a velocity of ~ 3.9 km/s observed by the conjugate stations cannot ideally confirm the true drift and distribution of EPIs in the flux tube with a velocity of ~ 0.1 km/s. The OTS delay in this place may be influenced by the fast motion of MEO satellites. However, using the S_4 data from geostationary Earth orbit (GEO) satellites (pseudo-random noise 135 and 138) observed by a meridional chain of receivers in South America, Shume and Mannucci (2013) also reported an obvious delay with various orders of scintillation occurrence in the flux tube, indicating the anisotropy of EPIs along the flux tube. One mechanism responsible for the asymmetry of EPIs could be associated with the asymmetry of EIA. During the generation stage of the irregularities, the asymmetry of EIA could reduce the instability growth rate through its control on *F* layer bottomside upward density gradients and the magnetic flux tube integrated conductivities (e.g., Abdu, 1997), thus resulting in the asymmetries in the ambient ionization and in the electron density gradients at latitudes adjacent to the EIA regions, which could be a possible cause for the EPI asymmetry (e.g., De Paula et al., 2010). However, in our study, the clear asymmetry of EIA in Figure 2a did not result in an obvious delay of scintillation occurrence as shown in Figure 3. A long time period statistics shown in Figures 10 and 11 indicated that the difference of scintillation OTS between two conjugate stations should be associated with their different local sunset time during the solar maximum years. Shume and Mannucci (2013) also pointed out that the local geophysical conditions, including the local density gradients, the current divergence, and the resulting polarization electric fields, and wind structures, should be conducive to generate plasma instabilities at each location along the flux tube.

The detailed mechanisms affecting the EPIs asymmetry along the flux tube need further investigation. Nevertheless, this study provides several interesting points in the investigation of geomagnetically conjugate distribution of EPIs. First, two ionospheric scintillation indexes, that is, ROTI (phase) and S_4 (amplitude), derived from common GNSS receivers instead of the dedicated ISMRs were established and used to investigate the EPIs. They would further advance the research of EPIs in regional and global scales. Second, for the first time, we presented a long time period statistics (2015–2017) of OTS in two hemispheres at the Africa

longitudes and reported the asymmetry of EPIs in the magnetic flux tube, indicating that the EPIs should not be equally distributed along the flux tube. In addition, during the solar maximum years, a close relationship between local sunset time and OTS associated with EPIs was also evidenced in this study.

5. Summary

In this work, we presented examples of EPIs using the in situ electron density measurements of the Swarm lower pair satellites and simultaneous GPS scintillation information (ROTI and S_4) derived from two geomagnetically conjugate ground stations, MAS1 (NH) and ASCG (SH), located at the Atlantic islands. The main findings can be summarized as follows:

1. EPIs are occasionally only observed in one hemisphere as indicated by the Swarm in situ electron density measurements. But in this situation, the GPS scintillations are still observed from the Swarm onboard receiver, as well as the two geomagnetically conjugate ground stations. It implies that the EPIs should generally elongate along the geomagnetic flux tube, but as Swarm probes plasma only along its orbit, it may miss detecting the finer structures of EPIs that are not equally distributed along the flux tube.
2. Statistical results indicate that the OTS in the NH is on average 16 and 18 min earlier than that in the SH for September equinox and December solstice in 2015, while for March equinox in 2016 the OTS of northern station is about 11 min later than that of southern station, which suggests the asymmetry features of EPIs along the flux tube.
3. Further with nearly three-year GPS data from two geomagnetically conjugate stations at the Asia longitudes, we find that the local sunset time plays an important role for causing the difference of OTS between two conjugate stations. Our results also suggest that this relationship is not remarkable during the minimum solar year.
4. In addition to the investigation of EPIs conjugacy, we also verified the availability of ionospheric scintillation indexes ROTI and S_4 , derived from common GNSS receiver, in EPIs study. Besides, compared to the ROTI index based on phase measurement, the amplitude scintillation index S_4 calculated by the C/N_0 measurement seems more sensitive to the receiver noise processing capability.

Acknowledgments

This work was supported by the National Key Research and Development Program of China (2017YFB0503401 and 2016YFB0501802). This work is also supported by the special funding of Wuhan University graduate study abroad exchange project. The European Space Agency (ESA) is acknowledged for providing the Swarm data. The official Swarm website is <http://earth.esa.int/Swarm>, and the server for Swarm data distribution is <ftp://Swarm-diss.eo.esa.int>. The authors would like to thank the MGEX data center CDDIS (<ftp://cddis.gsfc.nasa.gov/>) for providing GNSS data.

References

- Abdu, M. A. (1997). Major phenomena of the equatorial ionosphere-thermosphere system under disturbed conditions. *Journal of Atmospheric and Solar-Terrestrial Physics*, 59(13), 1505–1519. [https://doi.org/10.1016/S1364-6826\(96\)00152-6](https://doi.org/10.1016/S1364-6826(96)00152-6)
- Abdu, M. A. (2009). Major phenomena of the equatorial ionosphere-thermosphere system under disturbed conditions. *Journal of Atmospheric and Solar-Terrestrial Physics*, 59(13), 1505–1519. [https://doi.org/10.1016/S1364-6826\(96\)00152-6](https://doi.org/10.1016/S1364-6826(96)00152-6)
- Abdu, M. A., Batista, I. S., Reinisch, B. W., de Souza, J. R., Sobral, J. H. A., Pedersen, T. R., et al. (2009). Conjugate Point Equatorial Experiment (COPEX) campaign in Brazil: Electrodynamics highlights on spread F development conditions and day-to-day variability. *Journal of Geophysical Research*, 114, A04308. <https://doi.org/10.1029/2008JA013749>
- Aquino, M., Moore, T., Dodson, A., Waugh, S., Souter, J., & Rodrigues, F. S. (2005). Implications of ionospheric scintillation for GNSS users in northern Europe. *Journal of Navigation*, 58(2), 241–256. <https://doi.org/10.1017/S0373463305003218>
- Balan, N., Liu, L., & Le, H. (2018). A brief review of equatorial ionization anomaly and ionospheric irregularities. *Earth and Planetary Physics*, 2(4), 257–275. <https://doi.org/10.26464/epp2018025>
- Burke, W. J., Gentile, L. C., Huang, C. Y., Valladares, C. E., & Su, S. Y. (2004). Longitudinal variability of equatorial plasma bubbles observed by DMSP and ROCSAT-1. *Journal of Geophysical Research*, 109, A12301. <https://doi.org/10.1029/2004JA010583>
- Crane, R. K. (1997). Ionospheric scintillation. *IEEE*, 65(2), 180–199. Retrieved from http://www.nasa.gov/mission_pages/cindi/scintillation.html#.VGdhh_msU30
- De Paula, E. R., Muella, M. T. A. H., Sobral, J. H. A., Abdu, M. A., Batista, I. S., Beach, T. L., & Groves, K. M. (2010). Magnetic conjugate point observations of kilometer and hundred-meter scale irregularities and zonal drifts. *Journal of Geophysical Research*, 115, A08307. <https://doi.org/10.1029/2010JA015383>
- Friis-Christensen, E., Lühr, H., Knudsen, D., & Haagmans, R. (2008). Swarm—An Earth Observation Mission investigating Geospace. *Advances in Space Research*, 41(1), 210–216. <https://doi.org/10.1016/j.asr.2006.10.008>
- Fukushima, D., Shiokawa, K., Otsuka, Y., Nishioka, M., Kubota, M., Tsugawa, T., et al. (2015). Geomagnetically conjugate observation of plasma bubbles and thermospheric neutral winds at low latitudes. *Journal of Geophysical Research: Space Physics*, 120, 2222–2231. <https://doi.org/10.1002/2014JA020398>
- Gwal, A., Dubey, S., Wahi, R., & Feliziani, A. (2006). Amplitude and phase scintillation study at Chiang Rai, Thailand. *Advances in Space Research*, 38(11), 2361–2365. <https://doi.org/10.1016/j.asr.2006.02.057>
- Huba, J. D., Ossakow, S. L., Joyce, G., Krall, J., & England, S. L. (2009). Three-dimensional equatorial spread F modeling: Zonal neutral wind effects. *Geophysical Research Letters*, 36, L19106. <https://doi.org/10.1029/2009GL040284>
- Jiao, Y., Morton, Y. T., Taylor, S., & Pelgrum, W. (2013). Characterization of high-latitude ionospheric scintillation of GPS signals. *Radio Science*, 48, 698–708. <https://doi.org/10.1002/2013RS005259>
- Juan, J. M., Aragon-Angel, A., Sanz, J., González-Casado, G., & Rovira-García, A. (2017). A method for scintillation characterization using geodetic receivers operating at 1 Hz. *Journal of Geodesy*, 91(11), 1383–1397. <https://doi.org/10.1007/s00190-017-1031-0>

- Juan, J. M., Sanz, J., González-Casado, G., Rovira-Garcia, A., Camps, A., Riba, J., et al. (2018). Feasibility of precise navigation in high and low latitude regions under scintillation conditions. *Journal of Space Weather and Space Climate*, 8, 1–11. <https://doi.org/10.1051/swsc/2017047>
- Kelley, M. C. (1989). *The Earth's Ionosphere: Plasma Physics and Electrodynamics*. San Diego, CA: Academic Press, Inc.
- Kelley, M. C. (2009). *The Earth's Ionosphere: Electrodynamics and Plasma Physics* (2nd ed.). New York: Elsevier.
- Kil, H., Heelis, R. A., Paxton, L. J., & Oh, S. (2009). Formation of a plasma depletion shell in the equatorial ionosphere. *Journal of Geophysical Research*, 114, A11302. <https://doi.org/10.1029/2009JA014369>
- Kil, H., Paxton, L. J., & Oh, S. (2009). Global bubble distribution seen from ROCSAT-1 and its association with the evening prereversal enhancement. *Journal of Geophysical Research*, 114, A06307. <https://doi.org/10.1029/2008JA013672>
- Kintner, P. M., & Ledvina, B. M. (2004). Size, shape, orientation, speed, and duration of GPS equatorial anomaly scintillations. *Radio Science*, 39, RS2012. <https://doi.org/10.1029/2003RS002878>
- Knudsen, D. J., Burchill, J. K., Buchert, S. C., Eriksson, A. I., Gill, R., Wahlund, J. E., et al. (2017). Thermal ion imagers and Langmuir probes in the Swarm electric field instruments. *Journal of Geophysical Research: Space Physics*, 122, 2655–2673. <https://doi.org/10.1002/2016JA022571>
- Liu, K., Li, G., Ning, B., Hu, L., & Li, H. (2015). Statistical characteristics of low-latitude ionospheric scintillation over China. *Advances in Space Research*, 55(5), 1356–1365. <https://doi.org/10.1016/j.asr.2014.12.001>
- Lomidze, L., Knudsen, D. J., Burchill, J., Kouznetsov, A., & Buchert, S. C. (2018). Calibration and validation of swarm plasma densities and electron temperatures using ground-based radars and satellite radio occultation measurements. *Radio Science*, 53, 15–36. <https://doi.org/10.1002/2017RS006415>
- Luo, X., Lou, Y., Xiao, Q., Gu, S., Chen, B., & Liu, Z. (2018). Investigation of ionospheric scintillation effects on BDS precise point positioning at low-latitude regions. *GPS Solutions*, 22(63), 1–12. <https://doi.org/10.1007/s10291-018-0728-8>
- Martinis, C., & Mendillo, M. (2007). Equatorial spread *F*-related airglow depletions at Arecibo and conjugate observations. *Journal of Geophysical Research*, 112, A10310. <https://doi.org/10.1029/2007JA012403>
- Mendillo, M. (1997). Investigations of thermospheric-ionospheric dynamics with 6300-Å images from the Arecibo Observatory. *Journal of Geophysical Research*, 102(A4), 7331–7343. <https://doi.org/10.1029/96JA02786>
- Moreno, B., Radicella, S., de Lacy, M. C., Herraiz, M., & Rodriguez-Caderot, G. (2011). On the effects of the ionospheric disturbances on precise point positioning at equatorial latitudes. *GPS Solutions*, 15(4), 381–390. <https://doi.org/10.1007/s10291-010-0197-1>
- Otsuka, Y., Shiokawa, K., Ogawa, T., & Wilkinson, P. (2002). Geomagnetic conjugate observations of equatorial airglow depletions. *Geophysical Research Letters*, 29(15), 1753. <https://doi.org/10.1029/2002GL015347>
- Pi, X., Mannucci, A. J., Lindqwister, U. J., & Ho, C. M. (1997). Monitoring of global ionospheric irregularities using the worldwide GPS network. *Geophysical Research Letters*, 24(18), 2283–2286. <https://doi.org/10.1029/97GL02273>
- Shiokawa, K., Otsuka, Y., Ogawa, T., & Wilkinson, P. (2004). Time evolution of high-altitude plasma bubbles imaged at geomagnetic conjugate points. *Annales Geophysicae*, 22(9), 3137–3143. <https://doi.org/10.5194/angeo-22-3137-2004>
- Shume, E. B., & Mannucci, A. J. (2013). First calculation of phase and coherence of longitudinally separated L-band equatorial ionospheric scintillation. *Geophysical Research Letters*, 40, 3496–3501. <https://doi.org/10.1002/grl.50702>
- Sobral, J. H. A., Abdu, M. A., Pedersen, T. R., Castilho, V. M., Arruda, D. C. S., Muella, M. T. A. H., et al. (2009). Ionospheric zonal velocities at conjugate points over Brazil during the COPEX campaign: Experimental observations and theoretical validations. *Journal of Geophysical Research*, 114, A04309. <https://doi.org/10.1029/2008JA013896>
- Spogli, L., Alfonsi, L., Romano, V., de Franceschi, G., Joao Francisco, G. M., Hirokazu Shimabukuro, M., et al. (2013). Assessing the GNSS scintillation climate over Brazil under increasing solar activity. *Journal of Atmospheric and Solar-Terrestrial Physics*, 105–106, 199–206. <https://doi.org/10.1016/j.jastp.2013.10.003>
- Stolle, C., Lu, H., Rother, M., & Balasis, G. (2006). Magnetic signatures of equatorial spread *F* as observed by the CHAMP satellite. *Journal of Geophysical Research*, 111, A02304. <https://doi.org/10.1029/2005JA011184>
- Su, S., Liu, C. H., Ho, H. H., & Chao, C. K. (2006). Distribution characteristics of topside ionospheric density irregularities: Equatorial versus midlatitude regions. *Journal of Geophysical Research*, 111, A06305. <https://doi.org/10.1029/2005JA011330>
- Swarm document (2018). Swarm level 1b product definition. National Space Institute Technical University of Denmark, SW-RS-DSC-SY-007, Issue 5.22, 2018-08-24.
- Valladares, C. E., Meriwether, J. W., Sheehan, R., & Biondi, M. A. (2002). Correlative study of neutral winds and scintillation drifts measured near the magnetic equator. *Journal of Geophysical Research*, 107(A7), 1112. <https://doi.org/10.1029/2001JA000042>
- van den Ijssel, J., Forte, B., & Montenbruck, O. (2016). Impact of Swarm GPS receiver updates on POD performance. *Earth, Planets and Space*, 68(1), 85. <https://doi.org/10.1186/s40623-016-0459-4>
- van Dierendonck, A. J., Klobuchar, J., & Hua, Q. (1993). Ionospheric scintillation monitoring using commercial single frequency C/A code receivers. In *Proceedings of the ION GPS 1993* (pp. 1333–1342). Salt Lake City, UT: Institute of Navigation.
- Wan, X., Xiong, C., Rodriguez-Zuluaga, J., Kervalishvili, G. N., Stolle, C., & Wang, H. (2018). Climatology of the occurrence rate and amplitudes of local time distinguished equatorial plasma depletions observed by Swarm satellite. *Journal of Geophysical Research: Space Physics*, 123, 3014–3026. <https://doi.org/10.1002/2017JA025072>
- Weber, E. J., Brinton, H. C., Buchau, J., & Moore, J. G. (1982). Coordinated airborne and satellite measurements of equatorial plasma depletions. *Journal of Geophysical Research*, 87(12), 503–513. <https://doi.org/10.1029/JA087iA12p10503>
- Wu, K., Xu, J., Wang, W., Sun, L., Liu, X., & Yuan, W. (2017). Interesting equatorial plasma bubbles observed by all-sky imagers in the equatorial region of China. *Journal of Geophysical Research: Space Physics*, 122, 10,596–10,611. <https://doi.org/10.1002/2017JA024561>
- Xiong, C., Stolle, C., Lühr, H., Park, J., Fejer, B. G., & Kervalishvili, G. N. (2016). Scale analysis of equatorial plasma irregularities derived from Swarm constellation. *Earth, Planets and Space*, 68(121), 1–12. <https://doi.org/10.1186/s40623-016-0568-5>
- Xiong, C., Xu, J., Wu, K., & Yuan, W. (2018). Longitudinal thin structure of equatorial plasma depletions coincidentally observed by Swarm constellation and all-sky imager. *Journal of Geophysical Research: Space Physics*, 123, 1593–1602. <https://doi.org/10.1002/2017JA025091>
- Yang, Z., & Liu, Z. (2017). Investigating the inconsistency of ionospheric ROTI indices derived from GPS modernized L2C and legacy L2 P(Y) signals at low-latitude regions. *GPS Solutions*, 21(2), 783–796. <https://doi.org/10.1007/s10291-017-0568-3>
- Yokoyama, T., Fukao, S., & Yamamoto, M. (2004). Relationship of the onset of equatorial *F* region irregularities with the sunset terminator observed with the Equatorial Atmosphere Radar. *Geophysical Research Letters*, 31, L24804. <https://doi.org/10.1029/2004GL021529>
- Zakharenkova, I., Astafyeva, E., & Cherniak, I. (2016). GPS and in situ Swarm observations of the equatorial plasma density irregularities in the topside ionosphere. *Earth, Planets and Space*, 68(120), 1–11. <https://doi.org/10.1186/s40623-016-0490-5>
- Zhang, X., Wu, M., Liu, W., Li, X., Yu, S., Lu, C., & Wickert, J. (2017). Initial assessment of the COMPASS/BeiDou-3: New-generation navigation signals. *Journal of Geodesy*, 91(10), 1225–1240. <https://doi.org/10.1007/s00190-017-1020-3>